

Optimization of a Dicarboxylic Series for in Vivo Inhibition of Citrate Transport by the Solute Carrier 13 (SLC13) Family

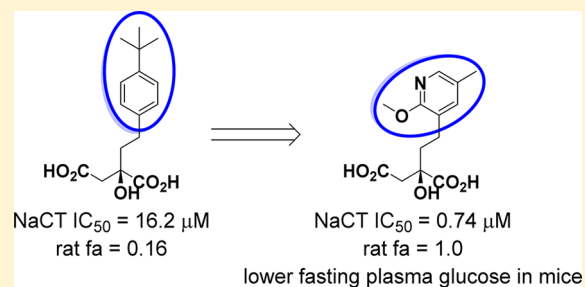
Kim Huard,^{*,†} James R. Gosset,[§] Justin I. Montgomery,^{||} Adam Gilbert,^{||} Matthew M. Hayward,^{||} Thomas V. Magee,[†] Shawn Cabral,^{||} Daniel P. Uccello,^{||} Kevin Bahnck,^{||} Janice Brown,[⊥] Julie Purkal,[‡] Matthew Gorgoglione,[‡] Adhiraj Lanba,[‡] Kentaro Futatsugi,[†] Michael Herr,^{||} Nathan E. Genung,^{||} Gary Aspnes,[†] Jana Polivkova,^{||} Carmen N. Garcia-Irizarry,^{||} Qifang Li,^{||} Daniel Canterbury,^{||} Mark Niosi,[⊥] Nicholas B. Vera,[‡] Zhenhong Li,[§] Bhagyashree Khunte,^{||} Jaclyn Siderewicz,^{||} Timothy Rolph,[‡] and Derek M. Erion^{*,‡}

[†]Worldwide Medicinal Chemistry, [‡]Cardiovascular, Metabolic and Endocrine Diseases Research Unit, and [§]Pharmacokinetics, Dynamics and Metabolism, Pfizer Worldwide Research & Development, Cambridge, Massachusetts 02139, United States

^{||}Worldwide Medicinal Chemistry, and [⊥]Pharmacokinetics, Dynamics and Metabolism, Pfizer Worldwide Research & Development, Groton, Connecticut 06340, United States

Supporting Information

ABSTRACT: Inhibition of the sodium-coupled citrate transporter (NaCT or SLC13A5) has been proposed as a new therapeutic approach for prevention and treatment of metabolic diseases. In a previous report, we discovered dicarboxylate **1a** (PF-06649298) which inhibits the transport of citrate in in vitro and in vivo settings via a specific interaction with NaCT. Herein, we report the optimization of this series leading to **4a** (PF-06761281), a more potent inhibitor with suitable in vivo pharmacokinetic profile for assessment of in vivo pharmacodynamics. Compound **4a** was used to demonstrate dose-dependent inhibition of radioactive [¹⁴C]citrate uptake in liver and kidney in vivo, resulting in modest reductions in plasma glucose concentrations.



INTRODUCTION

The SLC13 family comprises five family members, and three of these [*SLC13A2* (NaDC1), *SLC13A3* (NaDC3), and *SLC13A5* (NaCT)] co-transport di- and tricarboxylates with multiple sodium ions into cells.¹ Sodium-coupled sulfate transporters 1 and 2 (NaS1 and NaS2), respectively encoded by *SLC13A1* and *SLC13A4*, are not thought to be major transporters of dicarboxylates and tricarboxylates.^{1a,2} Sodium-coupled citrate transporter (NaCT) and sodium-coupled dicarboxylate transporters 1 and 3 (NaDC1 and NaDC3) are responsible for transporting cellular anionic intermediates such as citrate and succinate from the blood into the cells where these intermediates can serve as energy sources or intracellular signaling molecules.^{1c} More specifically, citrate can promote de novo lipogenesis (DNL) through polymerization of acetyl-CoA carboxylase (ACC)³ and promote the flux of glycolysis through allosteric interactions with phosphofructokinase (PFK).⁴ In human, the expression of *SLC13A5* is mostly restricted to liver, brain, and salivary glands, and NaCT primarily transports citrate into these tissues. *SLC13A2* and *SLC13A3* are expressed in kidney and intestine to regulate citrate excretion and absorption, respectively, but the expression of these two transporters is also detectable in other tissues. Unlike NaCT, NaDC1 and NaDC3 have a higher affinity for succinate over trianionic citrate.^{1c}

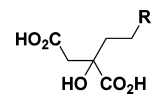
SLC13A5 is the predominant plasma citrate transporter expressed in human liver. Conversely, expression of *Slc13a2*, *Slc13a3*, and *Slc13a5* genes is detected in rodent liver in similar levels, where each contributes to hepatic citrate uptake.⁵ The exact contributions of NaDC1, NaDC3, and NaCT to citrate uptake in rodent liver are unknown, which complicates the pharmacodynamic translation of selective NaCT inhibition from rodent to human. Additionally, the biochemical kinetic characteristics of NaCT are different between rodents and human. In human, the transporter has high capacity but low citrate affinity compared to its rodent orthologue where the transporter has high affinity for citrate but significantly lower capacity than for human.^{1c,6}

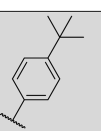
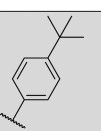
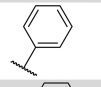
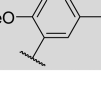
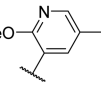
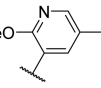
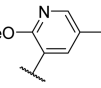
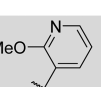
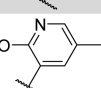
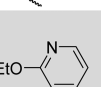
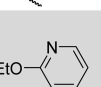
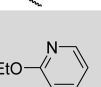
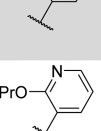
The whole-body knockout mouse of *Slc13a5* has been shown to promote a positive metabolic phenotype by increasing hepatic insulin responsiveness and reducing hepatic lipid burden through increasing cellular β -oxidation and reducing DNL in isolated hepatocytes.⁷ The inhibition of hepatic citrate uptake through inhibition of NaCT would benefit patients with metabolic diseases by reducing citrate flux into the liver and presumably exert the metabolic benefits through the modification of

Received: November 9, 2015

Published: January 6, 2016

Table 1. SAR Exploration of the Aryl Moiety To Improve Potency



Cpd	R	Stereocenter	HEK _{NaCT} IC ₅₀ ^a (μM)	Human hepatocytes IC ₅₀ ^a (μM)
1		Racemate	0.80 (6.1±0.4)	ND
1a		Eutomer (<i>R</i>) ^b	0.41 (6.4±0.3)	16.2 (4.8±0.1)
2		Racemate	>17	ND
3		Racemate	1.65 (5.8±0.2)	ND
4		Racemate	0.65 (6.5±0.2)	ND
4a		Eutomer	0.51 (6.3±0.3)	0.74 (6.1±0.1)
4b		Distomer	>18	ND
5		Racemate	3.37 (5.5±0.3)	ND
6		Racemate	0.19 (6.7±0.3)	ND
7		Racemate	0.11 (6.9±0.1)	ND
7a		Eutomer (<i>R</i>) ^b	0.11 (6.9±0.1)	0.33 (6.5±0.2)
7b		Distomer (<i>S</i>) ^b	>25	>30
8		Racemate	0.33 (6.5±0.2)	ND

^aIC₅₀ values are reported as geometric mean of at least three replicates with pIC₅₀ ± SD in parentheses. ^bConfigurations were assigned based on X-ray crystal analysis (Figure S1).¹⁰

intracellular metabolites.⁸ Nonselective SLC13 inhibitors have the potential to impact citrate flux in the kidney. The inhibition of renal citrate reuptake through blockade of NaDC1 and NaDC3 would increase renal citrate excretion with the potential to prevent calcium forming kidney stones, as they are often associated with reductions in urinary citrate output. The current therapy for reoccurring kidney stones is oral administration of citrate.⁹

We previously reported the identification of **1**, a small dicarboxylate capable of inhibiting the active transport of citrate in cells expressing NaCT (Table 1).¹⁰ This event is stereosensitive, as only the *R* enantiomer PF-06649298 (**1a**) showed activity in HEK-293-derived cells expressing NaCT (HEK_{NaCT}) and in cryopreserved cultured human hepatocytes (Figure 1).¹⁰

Enantiomer **1a** had an overall clean in vitro safety profile and showed selectivity within the SLC13 transporter family, as no inhibition of cellular citrate or succinate uptake was observed in cells expressing NaDC1 or NaDC3.¹⁰ Interestingly, data generated in whole cell experiments supported that **1a** is recognized as a substrate for active transport by NaCT, resulting in asymmetric distribution of compound in cells expressing NaCT. With acute treatment of **1a**, in vivo inhibition of hepatic citrate uptake was observed in mice. However, the limited exposure and potency of **1a** did not allow for extensive in vivo characterization of the mechanism and precluded clinical

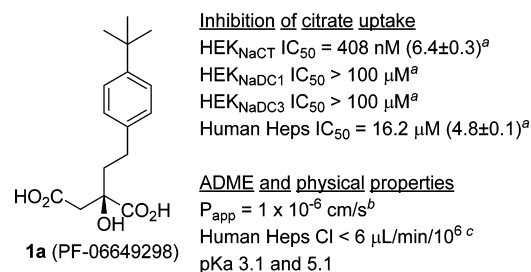
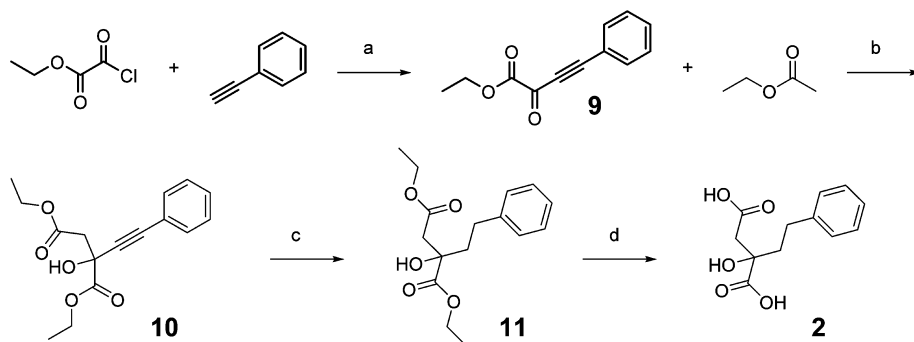
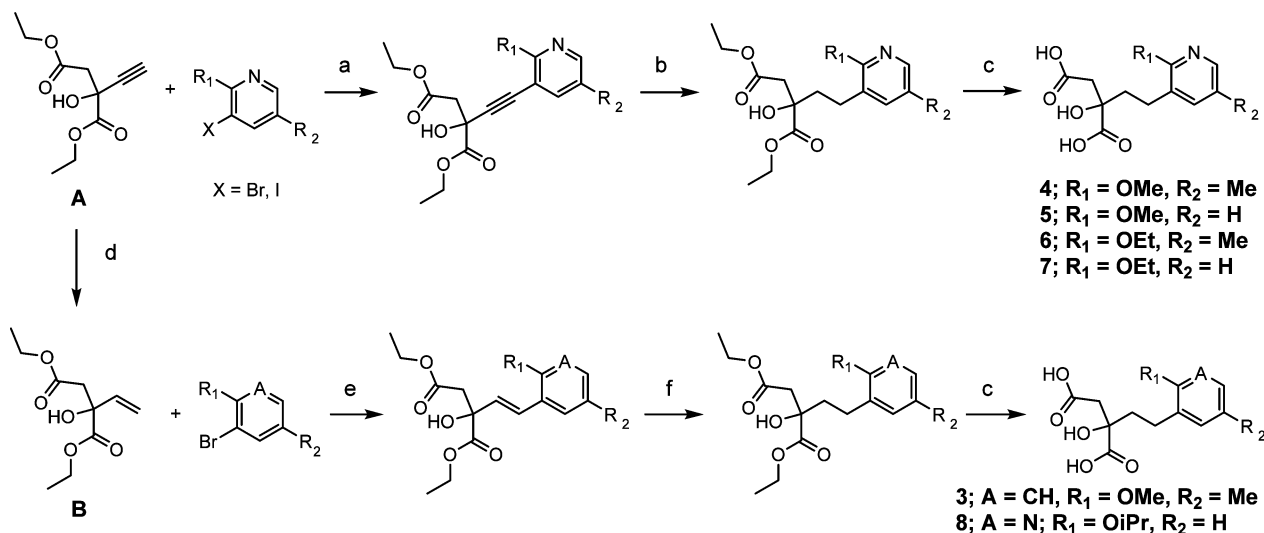


Figure 1. In vitro profile of compound **1a**. Active enantiomer **1a** inhibits cellular citrate uptake. Compound **1a** showed in vitro selectivity for NaCT over the dicarboxylate transporters NaDC1 and NaDC3 as well as undetectable clearance in human hepatocytes and low passive permeability. Footnotes: ^aInhibition of citrate uptake was measured in HEK-293 cells expressing NaCT, NaDC1, or NaDC3 as well as in cryopreserved human hepatocytes (Heps).¹⁰ IC₅₀ values are reported as geometric mean of at least three replicates with pIC₅₀ ± SD in parentheses. ^bPassive permeability (P_{app}) was assessed using MDCK-LE cell monolayer as described previously.¹¹ ^cIn vitro human hepatocyte clearance (Cl) was assessed as previously reported.¹²

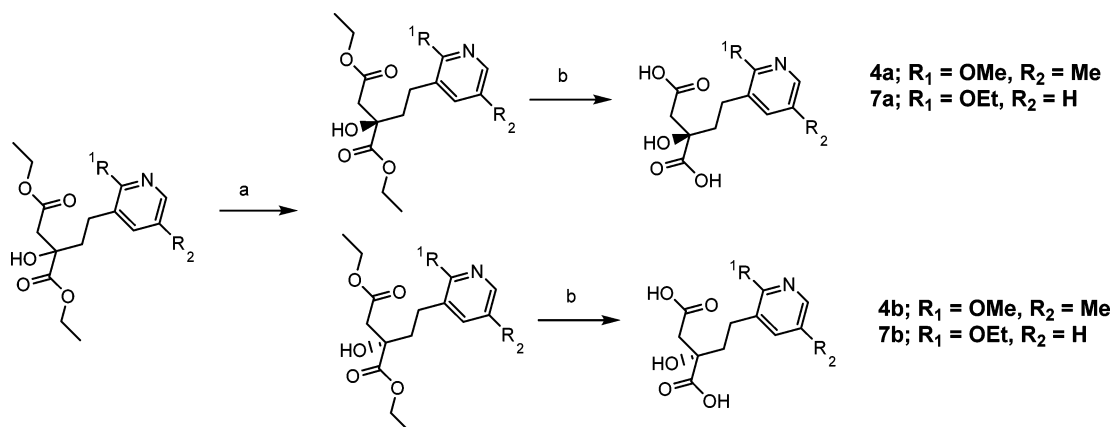
development. We therefore initiated a compound optimization effort with a focus on improving potency in human and rodent as well as pharmacokinetic (PK) properties. This report describes the challenges and progress made with this diacidic series as well as in vivo metabolic impact of these optimized compounds.

Scheme 1. Preparation of Dicarboxylate **2**^a

^aConditions: (a) CuI, TEA, THF, 50%; (b) LiHMDS, THF, 42%; (c) Pd/C, H₂, EtOH, 82%; (d) NaOH, THF, 74%.

Scheme 2. General Synthetic Scheme To Access **3–8**^a

^aConditions: (a) Pd(PPh₃)₂Cl₂, CuI, TEA, 29–91%; (b) Pd/C, EtOH, H₂ or Et₃SiH, 54–94%; (c) NaOH, EtOH, 5–96%; (d) Lindlar's catalyst, quinoline, toluene, H₂; (e) Pd(OAc)₂, P(Cy)₃, TEA, toluene, 110 °C; (f) Et₃SiH, MeOH, Pd/C, 30 °C.

Scheme 3. Synthesis of Enantiomers **4a,b** and **7a,b**^a

^aConditions: (a) chiral separation; (b) NaOH, THF, MeOH, 51–96%.

■ SYNTHESIS

The various dicarboxylates reported in this work were synthesized by general methods described in Schemes 1 and 2. Compound **2** was prepared by our previously reported methodology utilizing a copper-mediated coupling followed by

aldol addition and alkyne reduction.¹⁰ Final ester hydrolysis provided **2** as a racemic mixture (Scheme 1).

In order to quickly generate SAR around the aryl portion of the molecule, a synthetic sequence that allowed for late stage installation of various aryl groups was desired. The previously

Table 2. In Vivo Rat PK Properties of Dicarboxylates

compd	fu ^a	iv (1 mg/kg) ^b				po (5 mg/kg) ^c	
		total Cl _p (mL min ⁻¹ kg ⁻¹) ^d	renal Cl (mL min ⁻¹ kg ⁻¹) ^e	V _{dss} (L/kg)	T _{1/2} (h)	AUC _(0-∞) (ng·h/mL)	fa ^f
1	0.073	8.5	1.9 (3 × GFR)	0.45	1.2	1850	0.23
1a	0.054	4.5	0.5 (1 × GFR)	0.24	1.0	2570	0.16
4a	0.135	15.8	4.4 (4 × GFR)	0.54	1.7	4890	1.0
4b	0.058	9.9	2.8 (6 × GFR)	0.20	1.0	499	0.07
7a	0.086	6.7	1.8 (2 × GFR)	0.13	0.9	2650	0.24

^afu = fraction unbound as assessed by equilibrium dialysis.¹³ ^bVehicle: 10% DMSO/30% PEG400/60% water. ^cVehicle: 0.5% methylcellulose. ^dCl_p = plasma clearance. ^eMultiples of glomerular filtration rate (GFR) derived using GFR in the rat of 8.7 mL min⁻¹ kg⁻¹.¹⁴ ^fFraction of drug absorbed (fa) determined from AUC comparison following oral (po) and intravenous (iv) administration (method reported in the Supporting Information experimental section). The values calculated were comparable with values measured via portal vein cannulation for compounds 4a and 7a (Table S2).

reported terminal alkyne **A**¹⁰ played a critical role in preparation of compounds 3–8. Compounds 4–7 were synthesized by late stage aryl installation via Sonogashira coupling of **A** with the corresponding pyridyl halide, followed by alkyne reduction and ester hydrolysis (Scheme 2).

Low conversion with some aryl bromide substrates in the Sonogashira reaction led us to explore alternative methods for C–C bond formation. We found that Heck couplings with olefin **B** gave higher chemical yield in some cases.¹⁰ Reduction of alkyne **A** by hydrogenolysis using Lindlar's catalyst provided olefin **B** which led to compounds 3 and 8 via a Heck coupling, alkene reduction, and ester hydrolysis sequence. Enantiomers from corresponding racemic diethyl esters of 4 and 7 were separated by chiral HPLC to afford eutomers, 4a and 7a, and distomers, 4b and 7b, after final ester hydrolysis of enantiomerically pure diethyl esters (Scheme 3). The *R* configuration was assigned to 7a based on X-ray crystal analysis (Figure S1) and to 4a by analogy to 7a and 1a.¹⁰

RESULTS

One of our design objectives was to improve drug exposure of the diacidic series in rat. On the basis of preclinical in vivo PK profile of 1a, it was hypothesized that limited exposure of the compound was due to suboptimal absorption as a result of the low passive permeability (Figure 1). Compound 1a is a small hydrophilic molecule containing a hydroxysuccinic acid motif which is mostly in a dianionic form at physiological pH. These characteristics presumably confer low passive permeability to 1a, and our first objective was to improve passive permeability by modifying the polar hydroxysuccinic acid moiety while maintaining measurable activity in the cellular assay. Accordingly, a large number of analogs were prepared in which one of the carboxylic acid moieties was truncated or replaced with an uncharged functional group such as an amide, ester, alcohol, sulfone, or aryl ring. Even though some of these monocarboxylates demonstrated encouraging permeability, none of the analogs tested had measurable activity in the HEK_{NaCT} assay (data not shown), indicating the dicarboxylate motif is critical for inhibition. The hydroxyl group also proved to have an important function, since all modifications tested led to decreased potency. After several unsuccessful attempts to modify the polar fragment of the molecule, we concluded it would be beyond the scope of our efforts to achieve both acceptable passive permeability and measurable NaCT inhibitory activity with this series.

With our goal of identifying molecules that would enable rigorous in vivo testing of NaCT inhibition and given the critical role of the hydroxysuccinic acid motif, we focused on improving potency through optimization of the aryl moiety of the molecule

using the synthetic sequences depicted in Schemes 1 and 2. The presence of the hydroxysuccinic acid motif in all analogs generated with these methods results in polar molecules with passive permeability and metabolic clearance that were below or close to the limit of detection in our in vitro assays for all compounds in Table 1.

First, we established with compound 2 that substitution on the aryl ring is required for activity. As part of an exploratory library, the 2-methoxy 5-methyl substitution pattern of 3 was identified as a promising option with encouraging potency in the HEK_{NaCT} assay (Table 1). In compound 4, a nitrogen atom was incorporated in the aryl ring to influence the orientation of the ether group by creating electronic repulsion between the nitrogen and oxygen lone pairs. This was favorable for NaCT inhibition, and compound 4 inhibited the transport of citrate with potency comparable to that of analog 1 in the HEK_{NaCT} assay. Removal of the methyl group para to the methoxy substituent decreased potency 5-fold (Table 1, compounds 4 and 5). Interestingly, this SAR diverged with larger ethers, for which the activity was similar with or without the methyl group (Table 1, compounds 6 and 7). As exemplified with isopropoxy pyridine 8, larger ether substituents did not provide any benefit, and ethoxy pyridine 7 was the most potent analog to inhibit the uptake of citrate in the HEK_{NaCT} assay.

Consistent with our previous work, separation via chiral chromatography of 4 and 7 led to an active (4a and 7a) and an inactive enantiomer (4b and 7b), respectively. Unlike 1a, which appeared 40-fold less potent in human hepatocytes than in the HEK_{NaCT} cells (Table 1), eutomers 4a and 7a inhibited the cellular transport of citrate in both assays with similar potency (Table 1). The lack of activity for distomer 7b was confirmed in the human hepatocyte assay.

In spite of the low passive permeability associated with the dicarboxylates, we were encouraged by the exposure previously observed with 1a in mice¹⁰ and advanced 1, 1a, 4a, 4b as well as 7a to rat PK experiments (Table 2).

Consistent with their polar and acidic nature, analogs from this series had low-to-moderate total clearances, small volumes of distribution, and short half-lives. However, the fraction absorbed (fa) was variable and surprisingly high for such polar molecules. While racemate 1 and eutomer 1a were absorbed comparably, the fa for 4a was 14-fold higher than its enantiomer 4b (1.0 vs 0.07, Table 2). Despite its structural similarity to 4a, the PK profile obtained for 7a resembled that of 1a. Additionally, active renal secretion was observed to various degrees for this series. Overall, analog 4a offered an optimal balance of potency and oral exposure in rat and was subsequently profiled extensively (Figure 2).

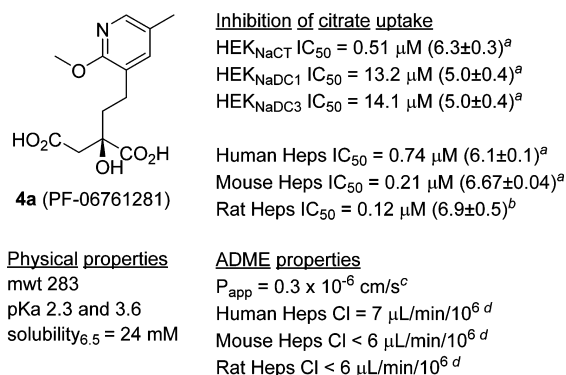


Figure 2. In vitro profile of **4a**. Compound **4a** is a small and polar dicarboxylate capable of potentially inhibiting the transport of citrate in rodent and human hepatocytes. It showed in vitro selectivity for NaCT over NaDC1 and NaDC3 as measured in HEK-293 cell systems and had low clearance in rodent and human hepatocytes, high aqueous thermodynamic solubility, and low passive permeability. The *R* configuration of **4a** was assigned by analogy to **1a** and **7a** (Figure S1). Footnotes: ^aInhibition of citrate uptake was measured in HEK-293 cells expressing NaCT, NaDC1, or NaDC3 as well as in cryopreserved human, mouse, and rat hepatocytes.¹⁰ IC₅₀ values are reported as a geometric mean of at least three replicates with pIC₅₀ ± SD in parentheses, unless otherwise noted. ^bThis IC₅₀ value was obtained from two replicates run in triplicate independent experiments. ^cPassive permeability was assessed using MDCK-LE cell monolayer as described previously.¹¹ ^dIn vitro human, mouse, and rat hepatocyte clearance.¹²

Compound **4a** was 20-fold more potent than our original hit **1a** for inhibition of citrate uptake in human hepatocytes (Table 1). In HEK-293 cells expressing NaDC1 or NaDC3, compound **4a** significantly inhibited both transporters with IC₅₀ values of approximately 14 μM. Despite its activity against NaDC1 and NaDC3, compound **4a** demonstrated >25-fold in vitro selectivity for NaCT within the SLC13 transporter family (Figure 2). Compound **4a** was inactive in a selectivity panel of 65 targets including the hERG channel, major human CYP450s as well as various transporters, ion channels, receptors, and enzymes (Table S1). With pK_a values of 2.3 and 3.6, a vast majority of **4a** is in the dianionic form at physiological pH resulting in favorable attributes, such as high aqueous solubility and low in vitro clearance in rat, mouse, and human hepatocytes (Figure 2). In addition to its acceptable PK profile in rat, **4a** inhibited the transport of citrate in mouse and rat hepatocytes with IC₅₀ values of 0.21 and 0.12 μM, respectively, and on this basis was selected for in vivo studies.

In order to assess the in vivo potency of **4a**, inhibition of radioactive citrate uptake was determined in selected tissues in Wistar Han rats. Radioactive [¹⁴C]citrate was administered intravenously to rats 3 h after the start of a constant infusion of **4a** via the carotid artery. Because of its short half-life, infusion was preferred over oral administration for **4a** in order to maintain a constant exposure for the duration of the study. In this setting, compound **4a** dose dependently reduced radioactive citrate uptake in liver, kidney, and testis with respective IC₅₀ values of 1.4, 1.0, and 1.0 μM (Figure 3).

Next, hyperinsulinemic–euglycemic clamps were performed to test the metabolic effects of blocking hepatic citrate uptake on glucose metabolism. Compound **4a** was infused into diet induced obese (DIO) mice to achieve a steady unbound exposure of 110-fold over the in vivo rat IC₅₀ (Figure S2). Potency of **4a** against citrate uptake was similar between rat and mouse hepatocytes, indicating minimal species difference. Prior to the start of the clamp, during the baseline portion of the drug infusion, **4a** modestly reduced fasting glucose concentrations (Figure 4A). In the hyperinsulinemic–euglycemic portion of the experiment, there was a trend for compound **4a** to increase the rate of glucose infusion in order to maintain euglycemia, but the changes did not reach statistical significance (Figure 4B).

Plasma unlabeled citrate concentrations were significantly increased during both the baseline and hyperinsulinemic–euglycemic portions of the experiment. During the hyperinsulinemic–euglycemic portion, uniformly ¹³C labeled [U-¹³C]-citrate was infused to characterize citrate kinetics and uptake. The plasma stable labeled citrate concentration was increased to the same degree as the nonlabeled citrate concentration in rats infused with compound **4a** (Figure 4C). Surprisingly, the hepatic concentrations of labeled and unlabeled citrate were also increased in the compound treated rats (Figure 4D). A similar observation of raised intracellular concentrations of citrate was made with human hepatocytes treated with **4a** (data not shown).

A potential explanation for the increase in intrahepatocyte concentration of citrate could be off-target inhibition of ATP citrate lyase; however there was no detectable inhibition of this enzyme at concentrations up to 30 μM in an isolated biochemical assay (Table S1). Furthermore, in an identical experiment to the described hyperinsulinemic–euglycemic clamp, a radioactive bolus of citrate was administered during the last 20 min of the clamp to confirm reductions in hepatic radioactive citrate uptake. Consistent with the reduction of radioactive citrate uptake during the exposure–response experiment using compound **4a** in rats (Figure 3), compound **4a** reduced hepatic radioactive

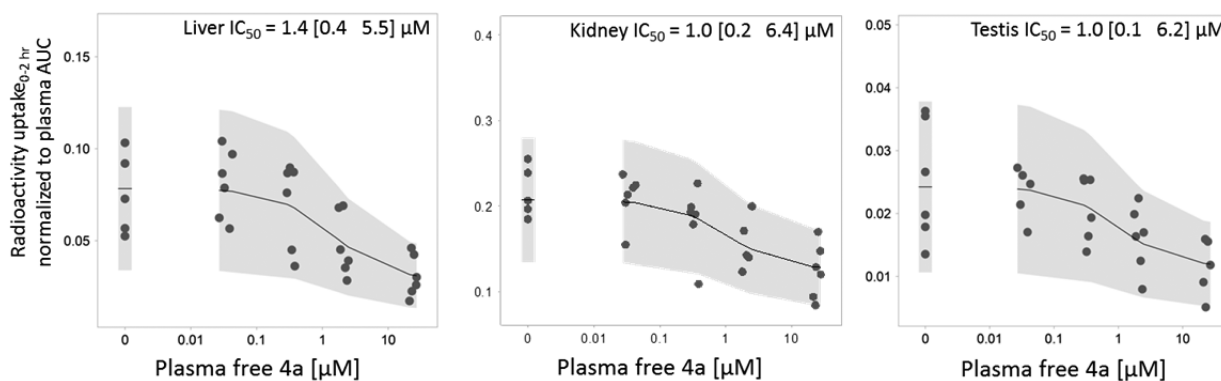


Figure 3. Exposure-dependent reductions in radioactive [¹⁴C]citrate uptake in liver, kidney, and testis normalized to the plasma radioactive AUC counts during an infusion with **4a**. IC₅₀ values were determined from plasma concentration of **4a** and reported with 95% confidence interval in parentheses.

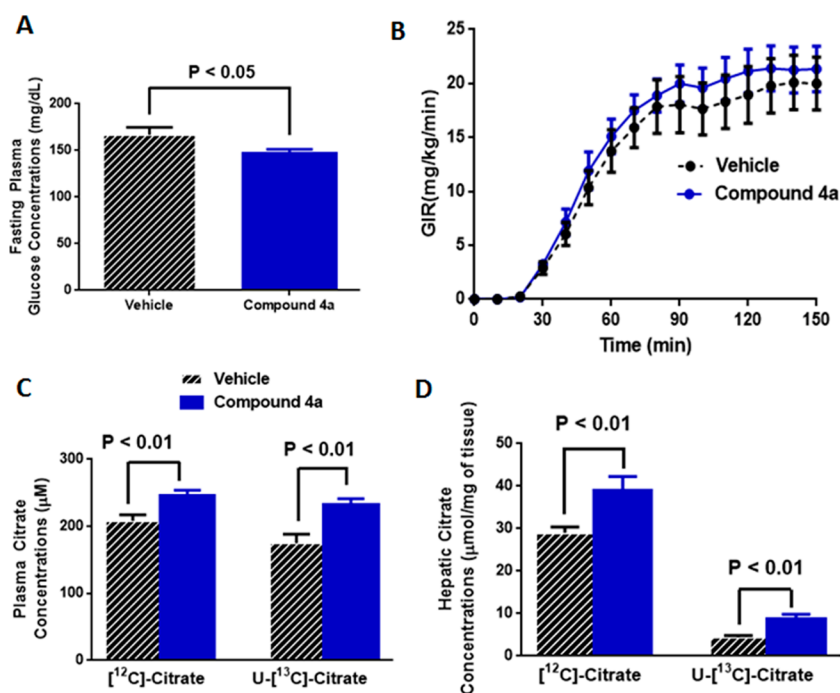


Figure 4. Effect of compound **4a** on glucose and citrate metabolism using the hyperinsulinemic–euglycemic clamp in DIO mice. (A) Plasma glucose concentrations during the basal portion. (B) Glucose infusion rate (GIR) needed to maintain euglycemia during the hyperinsulinemic–euglycemic clamp. (C) Plasma and (D) hepatic labeled [^{13}C] and unlabeled citrate concentrations at the end of the experiment. Data are the mean \pm SEM from 9 to 10 animals and were analyzed using one-way ANOVA followed by Tukey's multiple comparison test.

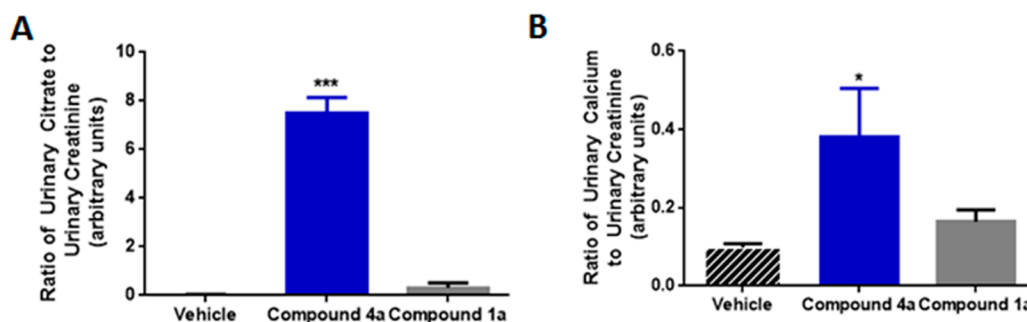


Figure 5. Effect of compounds **4a** and **1a** on urinary citrate and calcium output in mice. (A) Urinary citrate output and (B) calcium output normalized to creatinine. Data are the mean \pm SEM from 3 to 8 animals and were analyzed using one-way ANOVA followed by Tukey's multiple comparison test: (***) $P < 0.005$ vs vehicle, (*) $P < 0.05$ vs vehicle.

[^{14}C]citrate uptake during the hyperinsulinemic–euglycemic clamp in DIO mice (data not shown). These data support that treatment of rodents with **4a** inhibits the flux of citrate into the liver. As expected, this inhibition increases plasma citrate concentrations but paradoxically causes increases also in hepatic citrate concentrations.

Lastly, compounds **4a** and **1a** were orally administered at a 250 mg/kg dose in mice to test their effect on urinary citrate output (see Figure S3 for exposure). In mice treated with **4a**, urinary citrate was increased 230-fold over vehicle treated mice (Figure 5A). This is in contrast to the selective NaCT inhibitor **1a** which only caused the urinary citrate concentration to increase 10-fold (Figure 5A). Treatment with compound **4a** also caused an unexplained increase in urinary calcium (Figure 5B), and no changes in urinary sodium, volume, or pH were observed.

DISCUSSION AND CONCLUSION

As described in a previous report, the dicarboxylate series was identified from the Pfizer corporate compound collection by its

structural similarity to NaCT's endogenous substrate, citrate. More specifically, the 2-substituted 2-hydroxysuccinic acid motif is common to citrate and all active analogues from our series, as alterations to this moiety led to inactive analogues in our assay. Since an analog from the dicarboxylate series was previously shown to be a substrate for NaCT and to be competitive with citrate, the series likely shares a common binding site for which the 2-substituted 2-hydroxysuccinic acid moiety is an important recognition motif. As expected, the high-polarity, dianionic physicochemical properties conferred by the requisite hydroxysuccinic acid motif led to consistently low passive permeability. Although not commonly considered “druglike”, select analogues reported herein unexpectedly reached good exposure in rodents when dosed orally. One explanation for these results is that active transport played a role in gut absorption for some of the analogues. Consistent with this hypothesis, the fa of active enantiomer **4a** was 14 times greater than for the corresponding inactive enantiomer **4b**. Specific intestinal carriers were not identified for the transport of **4a**, but

the dicarboxylate transporters NaDC1 and NaDC3 may potentially play a role in the absorption. The recognition motif for transport appears to be strict, as a considerably smaller fraction of the dose was absorbed for the structurally similar analog **7a**. Owing to their small molecular weight and hydrophilic nature, paracellular absorption may be another route for the dicarboxylates to achieve moderate absorption.¹⁵ Similar and modest *fa* values were achieved after oral administration of compound **1** (racemic mixture) or **1a** (single enantiomer), suggesting a passive mode of absorption such as paracellular for some of the analogues. Renal clearance for most analogues evaluated *in vivo* was greater than rat GFR, implying active renal secretion, although no specific carriers were identified in this study. Not knowing which intestinal and renal transporters determine absorption and renal secretion of the dicarboxylates made it difficult to optimize the PK profile of this series, without relying heavily on *in vivo* PK screening. Additionally, human PK prediction would have been a challenge, since species differences in expression and activity profiles are known for some transporters, including NaDC1 and NaDC3. Nonetheless, to permit preclinical evaluation of the effect of inhibiting NaCT *in vivo*, optimization of the series with respect to potency led to **4a** which had sufficient hepatic exposure in rat relative to its *in vitro* potency.

Compound **4a** inhibited citrate uptake in both liver and kidney in rats (IC₅₀ of 1.4 and 1.0 μM, respectively). Since there was no detectable expression of NaCT in the kidney tissue,¹⁶ this result implies nonselective inhibition of citrate uptake. The *in vivo* IC₅₀ in rat (Figure 3) was generated using plasma drug concentrations of **4a** and not the local concentrations at the site of action. As shown in Figure S2, free concentrations of **4a** were higher in kidneys than in liver or plasma and may result in significant inhibition of citrate transport via renal NaDC1 and/or NaDC3 despite the weaker *in vitro* potency of **4a** against these transporters. These data imply that the *in vitro* selectivity of a dicarboxylate such as **4a** is a poor predictor of *in vivo* selectivity, without proper correction for local renal concentrations. In rat, qRT-PCR data indicate NaCT is the predominant citrate transporter in rodent testicular tissue and thus represents the *in vivo* potency for selective NaCT inhibition.¹⁶ The *in vivo* IC₅₀ of **4a** for testicular tissue was only slightly left-shifted compared to liver tissue (IC₅₀ of 1.0 and 1.4 μM, respectively). These data indicate only a small contribution of citrate uptake *in vivo* from NaDC1 and NaDC3 in rodent liver tissue; however this does not take into consideration compensatory flux from NaDC1 and NaDC3 during the inhibition of NaCT.

The modest but significant reductions in plasma glucose concentrations in the presence of **4a** are consistent with the data reported for compound **1a**.¹⁰ These data support an acute lowering of plasma glucose concentrations by reducing hepatic citrate uptake, through either reduced supply of carbon atoms or a secondary mechanism yet to be elucidated. The increase in plasma citrate concentration in the presence of **4a** during the hyperinsulinemic–euglycemic clamp is expected; however the increase in hepatic citrate concentrations (¹³C and ¹²C) came as a surprise. Since intracellular labeled citrate can only arise by transport into hepatocytes, the observed higher intracellular citrate concentration is unlikely to have arisen from a compensatory increase in the generation of intracellular citrate. The higher hepatic citrate concentrations cannot be explained by direct ATP-citrate lyase inhibition, since **4a** was inactive against ATP-citrate lyase. Nor can it be explained by increase in hepatic citrate uptake, since **4a** hepatic uptake of radioactive citrate was

reduced. In the *SLC13a5* whole-body knockout animals, hepatic citrate concentrations were not measured.⁷ The relationship between the reductions in plasma glucose with **4a** and the hepatic citrate concentrations is unclear. Further studies are necessary to elucidate the mechanism by which **4a** increased hepatic citrate concentrations and lowered plasma glucose concentrations.

The increased urinary citrate output would support the potential use of SLC13A2/3/5 inhibitors to redirect plasma citrate into urine. Kidney stones derived from calcium deposits are treated by the administration of oral citrate, which significantly increases urinary concentration of citrate. This is an effective treatment for dissolving kidney stones through chelating of calcium, thereby preventing reoccurrence of future kidney stones in most patients. However, while citrate therapy is cheap and effective, there are nocturnal periods during which urinary citrate concentration decreases due to the short half-life of citrate. In addition, citrate therapy is associated with uncomfortable gastrointestinal side effects. A SLC13A2/3/5 inhibitor should sustain urinary citrate output without any of these effects. Selective NaCT inhibitors increase urinary output of citrate, as do SLC13a2 knockout mice.¹⁷ Consistent with these studies, compound **4a** increased output of urinary citrate dramatically over vehicle-treated mice. However, through an unknown mechanism, compound **4a** also increased urinary calcium concentrations. The increased urinary calcium concentration would limit the efficacy of a SLC13A2/3/5 inhibitor for the treatment of kidney stones. One hypothesis to explain the increased calcium concentrations is that the local concentration of **4a** altered local acid–base balance within the kidney by blocking the conversion of citrate into bicarbonate within the kidney tubule.¹⁸ There were no overall changes in plasma calcium homeostasis, and parathyroid hormone concentrations were unchanged (data not shown) implying a change in calcium homeostasis at the level of the kidney.

In summary, optimization of the selective NaCT inhibitor **1a** led to compound **4a**. Compound **4a** displayed good PK profile in rat and increased potency for NaCT inhibition, albeit with lower selectivity against NaDC1 and NaDC3. Treatment with **4a** in rodent concentration-dependently reduced citrate uptake in liver, kidney, and testis, which resulted in modest improvement of glucose metabolism. The expected increase in plasma and urinary citrate concentrations was accompanied by unexplained increase in hepatic citrate concentration. Taken together, compound **4a** represents a novel inhibitor of the SLC13a2/3/5 family with partial selectivity for NaCT, over NaDC1, and NaDC3, which reduced citrate uptake in testis, kidney, and liver and increased concentrations of citrate in plasma and urine.

■ EXPERIMENTAL SECTION

Materials and Methods. Preparation of diethyl 2-ethynyl-2-hydroxysuccinate (**A**) was previously reported.¹⁰ All other chemicals, reagents, and solvents were purchased from commercial sources and used without further purification unless otherwise noted. ¹H NMR spectra were recorded with 400, 500, or 600 MHz spectrometer and are reported relative to residual undeuterated solvent signals. Data for ¹H NMR spectra are reported as follows: chemical shift (δ, ppm), multiplicity, coupling constant (Hz), and integration. The multiplicities are denoted as follows: s, singlet; d, doublet; t, triplet; q, quartet; spt, septet; m, multiplet; br s, broad singlet. Liquid chromatography–mass spectrometry (LC–MS) was performed on an Waters Acquity H-class system (Waters Atlantis C18 column, 4.6 mm × 50 mm, 5 μm; 95% water/acetonitrile linear gradient to 5% water/acetonitrile over 4 min, hold at 5% water/95% acetonitrile to 5.0 min, trifluoroacetic acid modifier (0.05%); flow rate of 2.0 mL/min). Silica gel chromatography

was performed using a medium pressure Biotage or ISCO system, and columns were prepackaged by various commercial vendors including Biotage and ISCO. All tested compounds were determined to be >95% pure by HPLC with UV peak detection at 215 nm. The terms “concentrated” and “evaporated” refer to the removal of solvent at reduced pressure on a rotary evaporator with a water bath temperature not exceeding 60 °C. The configuration of compounds **7b**, **4a**, and **4b** was assigned based on the X-ray crystal structure analysis of **7a**, supporting that the *R* enantiomers are active, which is in agreement with previously published work.¹⁰ Optical rotations are reported with concentration in g/mL with solvent used in parentheses.

General Procedure A (Parallel Format). *Step 1.* Lindlar's catalyst (20 mg, 0.075 mmol) was added to a solution of diethyl 2-ethynyl-2-hydroxysuccinate (**A**) (300 mg, 1.4 mmol) and quinoline (50 μ L, 0.42 mmol) in toluene (5 mL), and the mixture was stirred at 30 °C under H₂ atmosphere (15 psi) for 16 h. The reaction mixture was filtered and the filtrate concentrated to give diethyl 2-hydroxy-2-vinylsuccinate (**B**) (160 mg, 0.74 mmol, 53%). The resulting material was dissolved in toluene (6 mL, 0.125 M) and used without further purification.

Step 2. Selected aryl halide (0.20 mmol) and triethylamine (0.18 mL, 1.4 mmol) were added to the toluene solution of diethyl 2-hydroxy-2-vinylsuccinate (**B**) (1.6 mL, 0.20 mmol). Nitrogen was bubbled in the reaction mixture for 1 min. Palladium(II) acetate (4.5 mg, 20 μ mol) and tricyclohexylphosphine (5.6 mg, 20 μ mol) were added to the reaction mixture, and bubbling with nitrogen was continued for 1 min. The reaction vial was sealed and shaken at 130 °C for 16 h. The reaction mixture was concentrated under reduced pressure, and the resulting alkyne was purified by TLC.

Step 3. The alkene intermediate obtained in step 2 was dissolved in methanol (5 mL). Triethylsilane (0.12 mL, 0.75 mmol) and palladium on carbon (40 mg) were added to the solution, the reaction vial was sealed, and the mixture was shaken under nitrogen atmosphere at 30 °C for 16 h. The reaction mixture was filtered and the filtrate concentrated under reduced pressure.

Step 4. The material was dissolved in ethanol (0.80 mL), and 1 M solution sodium hydroxide (0.80 mL, 0.80 mmol) was added. The reaction mixture was stirred at 80 °C for 1 h. Ethanol was removed under reduced pressure, and 1 N hydrochloric acid was added to adjust the pH to ~1. The mixture was extracted with dichloromethane (3 \times 2 mL), and the combined organic layer was concentrated. The residue was purified by HPLC on a 21.2 mm \times 250 mm \times 8 μ m Phenomenex Gemini C18 column using a gradient of 26–46% acetonitrile in water containing 0.225% trifluoroacetic acid over 8 min at 30 mL/min with UV monitoring.

2-Hydroxy-2-phenethylsuccinic Acid (2). Diethyl 2-hydroxy-2-phenethylsuccinate (**11**) (150 mg, 0.51 mmol) was dissolved in THF (2 mL). 1 N sodium hydroxide (2.0 mL, 2.0 mmol) was added at room temperature. The mixture was stirred at room temperature for 16 h. Water (10 mL) was added to the reaction mixture which was extracted with ethyl acetate (2 \times 15 mL). The aqueous layer was acidified to a pH of 3 with 1 N HCl. The aqueous layer was extracted with ethyl acetate (2 \times 25 mL). The organic layer was dried over magnesium sulfate, filtered, and concentrated to give 2-hydroxy-2-phenethylsuccinic acid (**2**) (90 mg, 74%) as an off-white solid. ¹H NMR (400 MHz, DMSO-*d*₆) δ 7.29–7.25 (m, 2H), 7.18–7.15 (m, 3H), 5.05 (s, 1H), 2.77 (d, *J* = 15.6 Hz, 1H), 2.70 (td, *J* = 12.5, 5.6 Hz, 1H), 2.53 (d, *J* = 15.6 Hz, 1H), 2.41 (td, *J* = 12.5, 5.6 Hz, 1H), 1.92–1.83 (m, 2H); *m/z* = 236.8 [M – 1][–].

2-Hydroxy-2-(2-methoxy-5-methylphenethyl)succinic Acid (3). 2-Hydroxy-2-(2-methoxy-5-methylphenethyl)succinic acid (**3**) was prepared according to general procedure A in parallel format using 2-bromo-1-methoxy-4-methylbenzene (40 mg, 0.20 mmol). *m/z* = 281 [M – H][–].

2-Hydroxy-2-(2-(2-methoxy-5-methylpyridin-3-yl)ethyl)succinic Acid (4). Diethyl ester **13**, **13a** or **13b** (550 mg, 1.6 mmol), was dissolved in tetrahydrofuran (3 mL) and MeOH (1 mL). 3 M sodium hydroxide (2.2 mL, 6.6 mmol) was added and the mixture stirred at room temperature for 16 h. Water (20 mL) was added and the mixture extracted with a 1:2 mixture of ethyl acetate/heptane (24 mL). The aqueous layer was adjusted to pH of ~3 with 1 N HCl (3 mL) and washed with 20% isopropanol in dichloromethane (3 \times 60 mL). The

combined organic layer was dried over magnesium sulfate, filtered, and concentrated to give an off-white solid. The material was stirred in a 1:5 mixture of ethyl acetate/hexanes (6 mL) for 48 h during which the material crystallized and 2-hydroxy-2-(2-(2-methoxy-5-methylpyridin-3-yl)ethyl)succinic acid (**4**, **4a** or **4b**) was isolated as a white solid (233–320 mg, 51–70%) after filtration. Enantiomeric excess of **4a** and **4b** was determined by SFC using a 4.6 mm \times 250 mm \times 5 μ m Tech OJ-H column using a gradient of 5–60% isopropanol containing 0.2% trifluoroacetic acid/CO₂ over 10 min at 3.0 mL/min with monitoring at 210 nm. The configurations of **4a** and **4b** were assigned by analogy to **1a** and **7a**, whose configurations were assigned by X-ray crystal analysis (Figure S1).¹⁰

2-Hydroxy-2-(2-(2-methoxy-5-methylpyridin-3-yl)ethyl)succinic Acid (4). ¹H NMR (400 MHz, DMSO-*d*₆) δ 12.43 (br s, 2H), 7.98 (dd, *J* = 5.1, 2.0 Hz, 1H), 7.46 (dd, *J* = 7.2, 1.8 Hz, 1H), 6.88 (dd, *J* = 7.2, 4.9 Hz, 1H), 4.93 (br s, 1H), 4.31 (q, *J* = 7.0 Hz, 2H), 2.78 (d, *J* = 15.6 Hz, 1H), 2.58–2.71 (m, 1H), 2.54 (d, *J* = 16.0 Hz, 1H), 2.39 (td, *J* = 13.1, 4.7 Hz, 1H), 1.74–1.96 (m, 2H), 1.31 (t, *J* = 7.0 Hz, 3H); *m/z* = 282.3 [M – 1][–].

(R)-2-Hydroxy-2-(2-(2-methoxy-5-methylpyridin-3-yl)ethyl)succinic Acid (4a). Enantiomer **4a** eluted at 4.13 min with 99.7% ee. ¹H NMR (500 MHz, DMSO-*d*₆) δ 12.65 (br s, 1H), 12.20 (br s, 1H), 7.80 (d, *J* = 1.5 Hz, 1H), 7.30 (d, *J* = 2.0 Hz, 1H), 4.93 (br s, 1H), 3.81 (s, 3H), 2.77 (d, *J* = 15.7 Hz, 1H), 2.58–2.66 (m, 1H), 2.51–2.55 (m, 1H), 2.30–2.39 (m, 1H), 2.17 (s, 3H), 1.86 (dt, *J* = 4.8, 12.7 Hz, 1H), 1.79 (dt, *J* = 4.9, 12.7 Hz, 1H); *m/z* = 282.3 [M – 1][–]. [α]_D –0.5° (c 0.0733, MeOH).

(S)-2-Hydroxy-2-(2-(2-methoxy-5-methylpyridin-3-yl)ethyl)succinic Acid (4b). Enantiomer **4b** eluted at 3.89 min with 98.9% ee. ¹H NMR (500 MHz, DMSO-*d*₆) δ 12.65 (br s, 1H), 12.20 (br s, 1H), 7.79 (d, *J* = 1.5 Hz, 1H), 7.29 (d, *J* = 2.0 Hz, 1H), 4.92 (br s, 1H), 3.80 (s, 3H), 2.76 (d, *J* = 15.7 Hz, 1H), 2.56–2.65 (m, 1H), 2.50–2.55 (m, 1H), 2.28–2.37 (m, 1H), 2.16 (s, 3H), 1.85 (dt, *J* = 4.9, 12.7 Hz, 1H), 1.78 (dt, *J* = 4.9, 12.7 Hz, 1H); *m/z* = 282.3 [M – 1][–]. [α]_D 9.0° (c 0.0777, MeOH).

2-Hydroxy-2-(2-(2-methoxy-5-methylpyridin-3-yl)ethyl)succinic Acid (5). Diethyl 2-hydroxy-2-(2-(2-methoxy-5-methylpyridin-3-yl)ethyl)succinate (**15**) (190 mg, 0.58 mmol) was dissolved in THF (3 mL). 1 M sodium hydroxide (11.7 mL, 11.7 mmol) was added at room temperature. The mixture was stirred at room temperature for 32 h. The reaction mixture was extracted with ethyl acetate (3 \times 10 mL) and the aqueous layer concentrated. The residue was extracted with a 10:1 dichloromethane/methanol mixture (40 mL), and the organic layer was concentrated under reduced pressure. The residue was purified by prep-HPLC to provide 2-hydroxy-2-(2-(2-methoxy-5-methylpyridin-3-yl)ethyl)succinic acid (**5**) (7.2 mg, 4.6%) as a white solid. ¹H NMR (400 MHz, MeOD-*d*₄) δ 7.96 (d, *J* = 4.8 Hz, 1H), 7.49 (d, *J* = 6.4 Hz, 1H), 6.88 (dd, *J* = 7.2, 5.2 Hz, 1H), 3.93 (br s, 3H), 2.96 (d, *J* = 16.0 Hz, 1H), 2.76 (td, *J* = 12.7, 4.8 Hz, 1H), 2.67 (d, *J* = 16.0 Hz, 1H), 2.52 (td, *J* = 12.7, 4.8 Hz, 1H), 2.01 (td, *J* = 12.2, 4.4 Hz, 1H), 1.92 (dt, *J* = 12.2, 4.4 Hz, 1H); *m/z* = 270.8 [M + 1]⁺.

2-(2-(2-Ethoxy-5-methylpyridin-3-yl)ethyl)-2-hydroxysuccinic Acid (6). Diethyl 2-(2-(2-ethoxy-5-methylpyridin-3-yl)ethyl)-2-hydroxysuccinate (**17**) (55 mg, 0.16 mmol) was dissolved in ethanol (4 mL). 1 M potassium hydroxide (0.78 mL) was added at room temperature. The mixture was stirred at room temperature for 12 h. Water (20 mL) was added to the reaction mixture, and ethanol was removed under reduced pressure. 1 M HCl was added to the resulting aqueous solution to adjust the pH to ~5. The mixture was extracted with ethyl acetate (3 \times 50 mL), and the combined organic layer was concentrated. The residue was purified by prep-HPLC to provide 2-(2-(2-ethoxy-5-methylpyridin-3-yl)ethyl)-2-hydroxysuccinic acid (**6**) as a white solid (10 mg, 22%). ¹H NMR (400 MHz, MeOD-*d*₄) δ 7.75 (s, 1H), 7.35 (s, 1H), 4.30 (q, *J* = 7.2 Hz, 2H), 2.97 (d, *J* = 16.8 Hz, 1H), 2.77–2.67 (m, 2H), 2.55–2.47 (m, 1H), 2.23 (s, 3H), 2.04 (td, *J* = 4.8, 12.8 Hz, 1H), 1.91 (td, *J* = 12.4, 4.4 Hz, 1H), 1.39 (t, *J* = 7.2 Hz, 3H); *m/z* = 298.4 [M + 1]⁺.

2-(2-(2-Ethoxy-5-methylpyridin-3-yl)ethyl)-2-hydroxysuccinic Acid (7). Diethyl ester **19**, **19a** or **19b** (245 mg, 0.722 mmol), was dissolved in tetrahydrofuran (3 mL) and methanol (1 mL) at room temperature. 2 M

sodium hydroxide (1.5 mL, 3.0 mmol) was added to the solution, and the mixture was stirred at room temperature for 16 h. Water (20 mL) was added to the mixture and subsequently extracted with a 1:2 mixture of ethyl acetate/heptane (24 mL). The pH of the aqueous layer was adjusted to ~3 with 1 M HCl (3 mL). The aqueous layer was extracted with a 1:4 mixture of isopropanol/dichloromethane (3 × 60 mL). The combined organic layer was dried over magnesium sulfate, filtered, and concentrated under reduced pressure to afford 2-(2-(2-ethoxypyridin-3-yl)ethyl)-2-hydroxysuccinic acid (**7**) (152–195 mg, 75–96%) as a white solid. $m/z = 284.1$ $[M + 1]^+$. The configurations of **7a** and **7b** were assigned based on X-ray crystal analysis of **7a** (Figure S1).

(R)-2-(2-(2-Ethoxypyridin-3-yl)ethyl)-2-hydroxysuccinic Acid (7a). $^1\text{H NMR}$ (400 MHz, DMSO- d_6) δ 12.42 (br s, 2H), 7.97 (dd, $J = 2.0, 5.1$ Hz, 1H), 7.46 (dd, $J = 1.8, 7.2$ Hz, 1H), 6.87 (dd, $J = 4.9, 7.2$ Hz, 1H), 4.92 (br s, 1H), 4.30 (q, $J = 7.0$ Hz, 2H), 2.78 (d, $J = 15.6$ Hz, 1H), 2.63 (dt, $J = 4.7, 12.9$ Hz, 1H), 2.54 (d, $J = 15.6$ Hz, 1H), 2.39 (dt, $J = 4.9, 13.0$ Hz, 1H), 1.74–1.94 (m, 2H), 1.30 (t, $J = 7.0$ Hz, 3H); $m/z = 284.1$ $[M + 1]^+$. $[\alpha]_D -2.91^\circ$ (c 0.00755, MeOH).

(S)-2-(2-(2-Ethoxypyridin-3-yl)ethyl)-2-hydroxysuccinic Acid (7b). $^1\text{H NMR}$ (400 MHz, DMSO- d_6) δ 12.43 (br s, 2H), 7.98 (d, $J = 3.3$ Hz, 1H), 7.46 (d, $J = 5.9$ Hz, 1H), 6.88 (dd, $J = 5.1, 7.0$ Hz, 1H), 4.92 (br s, 1H), 4.31 (q, $J = 7.0$ Hz, 2H), 2.78 (d, $J = 15.6$ Hz, 1H), 2.59–2.70 (m, 1H), 2.56 (d, $J = 1.0$ Hz, 1H), 2.39 (dt, $J = 4.5, 12.9$ Hz, 1H), 1.75–1.96 (m, 2H), 1.31 (t, $J = 7.0$ Hz, 3H); $m/z = 284.1$ $[M + 1]^+$. $[\alpha]_D +2.70^\circ$ (c 0.0100, MeOH).

2-Hydroxy-2-(2-(2-isopropoxyppyridin-3-yl)ethyl)succinic Acid (8). 2-Hydroxy-2-(2-(2-isopropoxyppyridin-3-yl)ethyl)succinic acid (**8**) was prepared according to general procedure A in parallel format using 3-bromo-2-isopropoxyppyridine (43.0 mg, 0.20 mmol). $m/z = 296$ $[M - H]^-$.

Hepatocyte IC₅₀ Determination. Cryopreserved mouse, rat, or human hepatocytes were plated in a 48- or 96-well collagen-coated plate respectively at 50 000 cells/well in recovery/plating media (Corning 454534). The cells were allowed to attach to the plate for 3 h in an incubator at 37 °C under 5% CO₂. Subsequently, the medium was aspirated and replaced with Williams E medium supplemented with 100 nM dexamethasone, 1 × ITS+ (Corning, 354352), 1 × pen/strep, and 1 × L-glutamine and placed in an incubator at 37 °C under 5% CO₂ overnight. On the day of the experiment, compounds were added to the medium at the appropriate concentration and incubated for 30 min. Following the incubation step, citrate (pH = 7.4) was added to the hepatocytes as a mixture of unlabeled (Sigma-Aldrich) and 1 μCi 1,5- ^{14}C -labeled citrate (PerkinElmer NEC160250UC) resulting in the final concentration of 150 μM citrate per well. For the control background wells, 100 μL of RIPA buffer was added to the cells. The cells were incubated for 40 and 165 min for human and mouse hepatocytes, respectively. To stop the reaction, cells were washed with phosphate buffer saline (PBS), followed by the addition of 100 and 50 μL of RIPA buffer for mouse and human hepatocytes, respectively. For the human hepatocytes, 45 μL of the resulting solution was added to a PerkinElmer isoplate along with 200 μL of Optiphase Supermix (Perkin Elmer 1200-439). Subsequently, plates were analyzed by a PerkinElmer Microbeta Trilux scintillation counter. For the mouse hepatocytes, 95 μL of the resulting solution was added to a 7 mL glass scintillation vial along with 6 mL of Optiphase Supermix. Samples were analyzed on a Beckman Tri-Carb liquid scintillation counter.

Animals. All procedures and experiments involving animals were carried as per the protocols and guidelines reviewed and approved by Pfizer Institutional Animal Care and Use Committee. Male Wistar Han rats (approximately 200–300 g body weight) were purchased from Taconic Laboratories (Germantown, NY) when the in-life experiments were performed in-house or by contract lab BioDuro Inc. (Shanghai, China). Rats were housed one per cage in an American Animal Association Laboratory Animal Care accredited facility with a 12 h light/dark cycle (7:00 a.m. to 7:00 p.m.) and a mean temperature of 22 °C. This investigation conformed to the Guide for the Care and Use of Laboratory Animals published by the U.S. National Institutes of Health (NIH Publication No. 85-23, revised 1996). Rats were allowed to acclimate to their environment. Rats were fasted, for oral dosing groups,

overnight prior to dosing with free access to water. Food was administered 4 h postdose.

Pharmacokinetic Studies (Rat). Individual pharmacokinetic studies were conducted in male Wistar Han rats to determine plasma and/or urine exposures. For intravenous studies, rats received a single 1 mg/kg bolus dose of **1**, **1a**, **4a**, **4b**, or **7a** ($n = 2$ rats per compound), vehicle (10% DMSO/30% PEG400/60% water) at a dosing volume of 2 mL/kg. For oral studies, rats received a single 5 mg/kg dose of **1**, **1a**, **4a**, **4b**, or **7a** ($n = 2$ rats per compound), vehicle (0.5% methylcellulose) at a dosing volume of 10 mL/kg. Blood samples were collected via jugular venous catheter and placed into EDTA coated tubes, in a serial collection manner out to 24 h. Urine samples (iv only) were collected for 0–24 h. At the end of each time point, blood samples are temporarily placed on ice, then immediately centrifuged at 3500 rpm for 10 min. The resultant plasma samples were stored at –80 °C until LC–MS/MS analysis.

In Vivo IC₅₀. Carotid artery and jugular catheters were implanted into Sprague Dawley (SD) rats. Following a recovery period, the rats were fasted overnight for 16 h. At time 0, compound **4a** dissolved in 12% sulfobutyl ether β -cyclodextrin (SBECD) (rates: 77, 7.7, 0.7, or 0.07 mg $\text{kg}^{-1} \text{h}^{-1}$) or vehicle 12% SBECD was infused into the jugular vein. At 180 min, a 17.5 μCi ^{14}C citrate bolus was administered into the carotid artery. Plasma was collected at 185, 190, and 200 min following the radioactive bolus. At 200 min following the start of the infusion of **4a**, the rats were administered pentobarbital and liver, kidney, and testis were rapidly excised and freeze clamped in liquid nitrogen and stored at –80 °C until further analysis. For tissue radioactivity determination, 100–300 mg of tissue was homogenized in H₂O at a ratio of 1 mL/100 mg of tissue sample and placed in a 100 °C water bath for exactly 10 min. The samples were then centrifuged at 10 000 rpm for 30 min. 250 μL of the supernatant was added to 9 mL of ECOLite solution, and ^{14}C was counted using a scintillation counter.

Hyperinsulinemic–Euglycemic Clamp Studies. Male C57/B6 DIO (Jackson Laboratory) mice were acclimated for 10 days and kept on a 60% high-fat diet (D12492i; Research Diets). All the animals underwent right jugular vein catheterization surgery 1 week before the clamp study. Two catheters were implanted and exteriorized through a dorsal interscapular incision, then placed into a dorsal subcutaneous pocket. The mice were monitored on the heating pad after surgery until completely awake and then returned to their individual cages. Mice were treated with ketoprofen 2 mg/kg sc and ampicillin 100 mg/kg sc immediately before surgery. After a 7-day recovery period, mice were fasted for 16 h before the clamp and catheters were exteriorized at the end of the fasting period. Either compound **4a** (in 12% SBECD) or vehicle (12% SBECD) was infused (44 mg $\text{kg}^{-1} \text{h}^{-1}$) into the jugular vein. Following 90 min of compound infusion, blood was collected at –10 and 0 min for determination of fasting glucose concentrations. At time 0 min the variable glucose infusion (25% dextrose) and the 4 mU $\text{kg}^{-1} \text{min}^{-1}$ constant insulin infusion (with 0.3 mmol $\text{kg}^{-1} \text{h}^{-1}$ U- ^{13}C citrate) were started. Tail snip blood glucose was measured every 10 min, permitting glucose infusion rates to be adjusted according to each animal's glucose level until steady state was reached (~100 mg/dL). At time points 140 and 150 min blood was collected to determine plasma labeled and unlabeled citrate concentrations.

Citrate was extracted from 30 μL of rat plasma with methanol/formic acid (100:0.1, v/v) containing the following internal standard at a concentration of 10 μM : 2,2,4,4- ^2H citrate. The extract was diluted further with water/formic acid (100:0.1, v/v). Citrate was then analyzed by UPLC–MS/MS using a Waters Acquity UPLC coupled to a Sciex QTrap 5500 mass spectrometer. TCA cycle intermediates were separated by reversed phase chromatography on a Phenomenex Gemini C18 column, 3 μm , 150 mm × 3 mm. Citrate was then analyzed on the mass spectrometer using negative ion electrospray ionization in the multiple-reaction-monitoring mode. Liquid chromatogram peak integration was performed with Sciex MultiQuant software. All data reduction was performed with in-house software.

Urine Collection. Twenty-four 23-week-old C57BL/6J mice were purchased from Jackson Laboratories (Bar Harbor, ME). The animals were maintained on high fat diet (D12492i) from 6 weeks of age. Mice were treated with vehicle (0.5% methylcellulose in saline), 250 mg/kg of

compound **1a**, or 250 mg/kg of compound **4a**. Mice were placed into urine collection chambers immediately following dose, and animals were re-dosed with compounds after 7 h in chambers. Urine was collected for the full 24 h only in animals with measurable collected urine. Calcium concentrations were measured on a Siemens Advia 1800 platform (Siemens). Citrate was analyzed using the same protocol as above by replacing the plasma with 10 μ L of urine.

■ ASSOCIATED CONTENT

Supporting Information

The Supporting Information is available free of charge on the ACS Publications website at DOI: 10.1021/acs.jmedchem.5b01752.

Synthesis and characterization of all intermediates, in vitro selectivity data for **4a**, X-ray crystal structure of **7a**, fa assessment, exposure of compounds **1a** and **4a** for in vivo experiments (PDF)

Molecular formula strings (CSV)

■ AUTHOR INFORMATION

Corresponding Authors

*K.H.: phone, 1-617-522-3302; e-mail, Kim.Huard@Pfizer.com.

*D.M.E.: phone, 1-617-551-3755; e-mail, Derek.Erion@Pfizer.com.

Notes

The authors declare the following competing financial interest(s): All authors were employed by Pfizer during the completion and analysis of the studies herein reported.

■ ACKNOWLEDGMENTS

The authors thank Mark C. Noe, Mark E. Flanagan, Cesar A. de Oliveira, Kun Song, Jeremy Starr, Brandon Schuff, Marina Shalaeva, David Price, Robert Depianta, Gregory Ciszewski, Yimin Zhu, Qingyun Yan, Yingjiang Zhou, Ronald W. Clark, Charles Rotter, and Brian Samas for their contributions to the project.

■ ABBREVIATIONS USED

SLC13, solute carrier 13; NaS1, sodium-coupled sulfate transporter 1; NaS2, sodium-coupled sulfate transporter 2; NaCT, sodium-coupled citrate transporter; NaDC1, sodium-coupled dicarboxylate transporter 1; NaDC3, sodium-coupled dicarboxylate transporter 3; DNL, de novo lipogenesis; ACC, acetyl-CoA carboxylase; PFK, phosphofructokinase; HEK_{NaCT}, HEK-293-derived cells expressing NaCT; HEK_{NaDC1}, HEK-293-derived cells expressing NaDC1; HEK_{NaDC3}, HEK-293-derived cells expressing NaDC3; Heps, hepatocytes; P_{app} , apparent passive permeability; Cl, clearance; PK, pharmacokinetic; TEA, triethylamine; THF, tetrahydrofuran; LiHMDS, lithium hexamethylsilylazide; P(Ph)₃, triphenylphosphine; P(Cy)₃, tricyclohexylphosphine; fu, fraction unbound; GFR, glomerular filtration rate; iv, intravenous; po, oral administration; V_{dss} , steady state volume of distribution; $T_{1/2}$, half-life; AUC, area under the curve; fa, fraction absorbed; DMSO, dimethylsulfoxide; GFR, glomerular filtration rate; hERG, human ether-a-go-go-related gene; CYP450, cytochrome P450; mwt, molecular weight; DIO, diet induced obese; LC-MS, liquid chromatography-mass spectrometry; TLC, thin layer chromatography

■ REFERENCES

(1) (a) Bergeron, M. J.; Cl  men  on, B.; Hediger, M. A.; Markovich, D. SLC13 family of Na⁺-coupled di- and tri-carboxylate/sulfate trans-

porters. *Mol. Aspects Med.* **2013**, *34*, 299–312. (b) Markovich, D.; Murer, H. The SLC13 gene family of sodium sulphate/carboxylate cotransporters. *Pfluegers Arch.* **2004**, *447*, 594–602. (c) Pajor, A. M. Sodium-coupled dicarboxylate and citrate transporters from the SLC13 family. *Pfluegers Arch.* **2014**, *466*, 119–130.

(2) Lee, A.; Dawson, P. A.; Markovich, D. NaSi-1 and Sat-1: Structure, function and transcriptional regulation of two genes encoding renal proximal tubular sulfate transporters. *Int. J. Biochem. Cell Biol.* **2005**, *37*, 1350–1356.

(3) Gregolin, C.; Ryder, E.; Kleinschmidt, A. K.; Warner, R. C.; Lane, M. D. Molecular characteristics of liver acetyl CoA carboxylase. *Proc. Natl. Acad. Sci. U. S. A.* **1966**, *56*, 148–155.

(4) Garland, P. B.; Randle, P. J.; Newsholme, E. A. Citrate as an intermediary in the inhibition of phosphofructokinase in rat heart muscle by fatty acids, ketone bodies, pyruvate, diabetes, and starvation. *Nature* **1963**, *200*, 169–170.

(5) Yodoya, E.; Wada, M.; Shimada, A.; Katsukawa, H.; Okada, N.; Yamamoto, A.; Ganapathy, V.; Fujita, T. Functional and molecular identification of sodium-coupled dicarboxylate transporters in rat primary cultured cerebrocortical astrocytes and neurons. *J. Neurochem.* **2006**, *97*, 162–173.

(6) Zwart, R.; Peeva, P. M.; Rong, J. X.; Sher, E. Electrophysiological characterization of human and mouse sodium-dependent citrate transporters (NaCT/SLC13A5) reveal species differences with respect to substrate sensitivity and cation dependence. *J. Pharmacol. Exp. Ther.* **2015**, *355*, 247–254.

(7) Birkenfeld, A. L.; Lee, H. Y.; Guebre-Egziabher, F.; Alves, T. C.; Jurczak, M. J.; Jornayvaz, F. R.; Zhang, D.; Hsiao, J. J.; Martin-Montalvo, A.; Fischer-Rosinsky, A.; Spranger, J.; Pfeiffer, A. F.; Jordan, J.; Fromm, M. F.; K  nig, J.; Lieske, S.; Carmean, C. M.; Frederick, D. W.; Weismann, D.; Knauf, F.; Irusta, P. M.; De Cabo, R.; Helfand, S. L.; Samuel, V. T.; Shulman, G. I. Deletion of the mammalian INDY homolog mimics aspects of dietary restriction and protects against adiposity and insulin resistance in mice. *Cell Metab.* **2011**, *14*, 184–195.

(8) Rogers, R. P.; Rogina, B. The role of INDY in metabolism, health and longevity. *Front. Genet.* **2015**, *6*, 204.

(9) (a) Hamm, L. L.; Hering-Smith, K. S. Pathophysiology of hypocitraturic nephrolithiasis. *Endocrinol. Metab. Clin. North Am.* **2002**, *31*, 885–893. (b) Pak, C. Y. C.; Fuller, C.; Sakhaee, K.; Preminger, G. M.; Britton, F. Long-term treatment of calcium nephrolithiasis with potassium citrate. *J. Urol.* **1985**, *134*, 11–19.

(10) Huard, K.; Brown, J.; Jones, J. C.; Cabral, S.; Futatsugi, K.; Gorgoglione, M.; Lanba, A.; Vera, N. B.; Zhu, Y.; Yan, Q.; Zhou, Y.; Vernochet, C.; Riccardi, K.; Wolford, A.; Pirman, D.; Niosi, M.; Aspnes, G.; Herr, M.; Genung, N. E.; Magee, T. V.; Uccello, D. P.; Loria, P.; Di, L.; Gosset, J. R.; Hepworth, D.; Rolph, T.; Pfefferkorn, J. A.; Erion, D. M. Discovery and characterization of novel inhibitors of the sodium-coupled citrate transporter (NaCT or SLC13A5). *Sci. Rep.* **2015**, *5*, 17391–17403.

(11) Di, L.; Whitney-Pickett, C.; Umland, J. P.; Zhang, H.; Zhang, X.; Gebhard, D. F.; Lai, Y.; Federico, J. J., 3rd; Davidson, R. E.; Smith, R.; Reyner, E. L.; Lee, C.; Feng, B.; Rotter, C.; Varma, M. V.; Kempshall, S.; Fenner, K.; El-Kattan, A. F.; Liston, T. E.; Troutman, M. D. Development of a new permeability assay using low-efflux MDCKII cells. *J. Pharm. Sci.* **2011**, *100*, 4974–4985.

(12) Di, L.; Keefer, C.; Scott, D. O.; Strelevitz, T. J.; Chang, G.; Bi, Y.-A.; Lai, Y.; Duckworth, J.; Fenner, K.; Troutman, M. D.; Obach, R. S. Mechanistic insights from comparing intrinsic clearance values between human liver microsomes and hepatocytes to guide drug design. *Eur. J. Med. Chem.* **2012**, *57*, 441–448.

(13) Banker, M. J.; Clark, T. H.; Williams, J. A. Development and validation of a 96-well equilibrium dialysis apparatus for measuring plasma protein binding. *J. Pharm. Sci.* **2003**, *92*, 967–974.

(14) Lin, J. H. Species similarities and differences in pharmacokinetics. *Drug Metab. Dispos.* **1995**, *23*, 1008–1021.

(15) El-Kattan, A.; Hurst, S.; Brodfuehrer, J.; Loi, C.-M. Anatomical and physiological factors affecting oral drug bioavailability in rats, dogs, and humans. In *Oral Bioavailability: Basic Principles, Advanced Concepts*,

and Applications; Hu, M., Li, X., Eds.; John Wiley & Sons: Hoboken, NJ, U.S., 2011; pp 253–265, DOI: [10.1002/9781118067598.ch16](https://doi.org/10.1002/9781118067598.ch16).

(16) Inoue, K.; Zhuang, L.; Maddox, D. M.; Smith, S. B.; Ganapathy, V. Structure, function, and expression pattern of a novel sodium-coupled citrate transporter (NaCT) cloned from mammalian brain. *J. Biol. Chem.* **2002**, *277*, 39469–39476.

(17) Ho, H. T. B.; Ko, B. C. B.; Cheung, A. K. H.; Lam, A. K. M.; Tam, S.; Chung, S. K.; Chung, S. S. M. Generation and characterization of sodium-dicarboxylate cotransporter-deficient mice. *Kidney Int.* **2007**, *72*, 63–71.

(18) Zacchia, M.; Preisig, P. Low urinary citrate: An overview. *J. Nephrol.* **2010**, *23* (Suppl.16), S49–S56.